JOURNAL OF CATALYSIS 142, 182–197 (1993)

Role of Ammonia Oxidation in Selective Catalytic Reduction of Nitric Oxide over Vanadia Catalysts[1]

UMIT S. OZKAN,[2] YEPING CAI, MAHESH W. KUMTHEKAR, AND LIPING ZHANG

Department of Chemical Engineering, The Ohio State University, Columbus, Ohio 43210

Received November 23, 1992; revised February 26, 1993

The role of direct oxidation of ammonia in SCR reactions and the catalytic anisotropy of V_2O_5 catalysts in this reaction network were investigated. The catalysts were characterized using BET surface area measurement, X-ray diffraction, laser Raman spectroscopy, X-ray photoelectron spectroscopy, scanning electron microscopy, and 3-D imaging. Temperature-programmed reduction experiments using ammonia and hydrogen as reducing agents and temperature-programmed desorption studies were also performed. A steady-state fixed-bed reactor system was used for activity and selectivity measurements. The product analysis was carried out by a combination of techniques including chemiluminescence NO_x analysis, on-line gas chromatography and on-line mass spectrometry, and chemical titration methods. The results obtained in this study, when combined with our previous studies in SCR reactions, indicate that over vanadium pentoxide catalysts, ammonia oxidation and NO reduction reactions are closely coupled. The results suggest that ammonia adsorption takes place on at least two types of sites located on the (010) and (100) planes of V_2O_5. The sites that selectively reduce NO to N_2 are the V–O–V sites located on the side planes, whereas V=O sites promote direct oxidation of ammonia to NO and the formation of N_2O from NO and NH_3 interaction more readily. It is found that the V=O sites are more easily reduced with both hydrogen and ammonia.

INTRODUCTION

Selective catalytic reduction (SCR) is recognized as an effective postcombustion control technique to reduce NO_x emissions from chemical plants and stationary combustion sources. Vanadia-based catalysts have been proven to be quite effective in selectively reducing NO_x with ammonia and are being commercially used. The past decade has seen extensive work done on supported vanadia catalysts (*1–9*). Most of the work in this area has been summarized in some recent reviews (*10, 11*). Especially some of the more recent studies on this subject have shed considerable light on the SCR activity of vanadia catalysts supported on titania (*12–14*). In spite of their obvious importance and the large number of studies conducted over these catalysts, questions still remain about the nature of active sites that lead to selective reduction of NO or direct oxidation of ammonia.

In our earlier studies, we examined the activity and selectivity of vanadia catalysts on both anatase and rutile phases of titania support (*15, 16*). In our more recent work, we have examined the morphological aspects of the unsupported vanadia catalysts in selective catalytic reduction of NO (*17*). V_2O_5 catalysts have been reported to be structure sensitive in various reactions (*18–20*). Catalyst samples which preferentially exposed different crystallographic planes were obtained by using various thermal treatment techniques. These studies demonstrated the existence of catalytic anisotropy in SCR reactions over V_2O_5 crystals. These studies also indicated that direct oxidation of ammonia became important at

[1] *Disclaimer.* Any opinions, findings, and conclusions or recommendations expressed in this publication are those of the authors and do not necessarily reflect the views of the EPA.

[2] To whom correspondence should be addressed.

0021-9517/93 $5.00

higher temperatures. The main purpose of the present study is to investigate the ammonia oxidation reaction independently and to correlate the findings with the results of the SCR reactions performed over the same catalysts.

Ammonia oxidation reaction has been used in the industry for a long time for the production of nitric acid. Ammonia oxidation has been studied by many researchers over various catalysts as either a primary reaction (*21–26*) or as a side reaction (*5, 27*). The fact that nitric oxide is one of the major intermediates of this reaction makes its involvement in SCR reaction even more important. We believe that the selectivity of the SCR reaction cannot be considered alone without investigating the role played by the direct oxidation of ammonia.

In the present study, direct oxidation of ammonia was studied over the same temperature range as that of SCR reaction experiments in our previous work (*17*) using V_2O_5 catalysts preferentially exposing different crystal planes. Catalysts were characterized using BET surface area measurement, X-ray diffraction, scanning electron microscopy, 3-D imaging, X-ray photoelectron spectroscopy, and laser Raman spectroscopy. Temperature-programmed reduction studies were performed over catalyst samples using both ammonia and hydrogen as reducing agents. Temperature-programmed desorption of ammonia was also performed. The results from catalyst characterization, thermal analysis experiments, and ammonia oxidation studies have been combined with the results from selective catalytic reduction studies to acquire a better understanding of the nature of active sites that play a role in controlling the selectivity of the SCR reaction.

EXPERIMENTAL

Catalyst Preparation

Vanadium pentoxide crystals preferentially exposing different crystal planes were grown using thermal treatment techniques. The first of the two samples which are referred to in this paper, V_2O_5-D, was prepared by calcining ammonium metavanadate (Aldrich) at 520°C for 50 h in a flow of oxygen and was in the form of thick, almost cylindrical particles. The second sample, V_2O_5-M, was prepared by melting vanadium pentoxide (Aldrich, 99.6% pure) at 695°C for 2 h and then subjecting it to temperature-programmed cooling for recrystallization. This sample was gently broken into smaller pieces. Both samples were sieved for uniform particle size distribution and used in the reactor without pelletizing. The specific surface areas of V_2O_5-D and V_2O_5-M were 3.4 and 0.25 m^2/g, respectively. V_2O_5-M crystals which were broken into smaller size particles had a surface area of 1.0 m^2/g.

Catalyst Characterization

The specific surface areas of the catalysts were measured using BET technique with a Micromeritics 2100 E Accusorb instrument. Krypton was used as the adsorbent. X-ray powder diffraction patterns were obtained using a Scintag PAD V diffractometer. Cu K_α radiation (λ = 1.5432 Å) was used as the incident X-ray source. The surface morphology of the catalysts was examined through a Hitachi S-510 scanning electron microscope using a voltage of 25 kV and magnifications ranging from 100 to 8000×. 3-D Imaging was used in combination with the SEM studies to quantify the surface dimensions of the particles. The catalyst samples were also characterized using two laser Raman spectrometers (SPEX 1403 Ramalog 9-I Spectrometer and SPEX 1877 Triplemate Raman spectrometer) which used 5-W Argon ion lasers (Spectra Physics, Model 2016 and Model 2017) as the excitation source. X-ray photoelectron spectra of the samples were obtained using a Physical Electronics/Perkin–Elmer (Model 550) ESCA/Auger spectrometer, operated at 15 kV and 20 mA. The X-ray source was Mg K_α radiation (1253.6 eV). The binding energy of C 1*s* (284.6 eV) was used as a reference in these measurements. Details of the charac-

terization experiments have been presented previously (*17*).

Reaction Studies

Ammonia oxidation experiments were performed using a steady-state reactor system which was described previously (*17*). The feed gases (Linde) consisted of 0.53% NH_3 in He, 10% O_2 in He, and pure He. The gas flow rates were adjusted using three mass flow controllers (Tylan model FC-280) and a 4-channel readout box (Tylan model RO-28).

Analyses of feed and product streams were performed by combining gas chromatography, chemiluminescence and titration techniques. Inlet and outlet concentrations of nitric oxide and nitrogen dioxide (if present) were obtained with an on-line chemiluminescence NO–NO_x analyzer (Thermo environmental Instruments, Model 10) which includes a high-temperature converter for nitrogen dioxide and ammonia, and a low-temperature catalytic converter (Model 300) for nitrogen dioxide. The ammonia concentrations in the feed and the product streams were determined by a conventional titration method with the aid of hydrochloric acid solution of known concentration after ammonia was absorbed in diluted aqueous boric acid solution. An on-line gas chromatograph (Hewlett–Packard 5890 A) with a 10-ft Porapak Q column and an 8-ft molecular sieve 5A column, connected in series by a 4-port Valco column isolation valve, was used to quantify O_2, N_2, and N_2O concentrations.

Activity measurements were performed using a feed mixture that consisted of 1418 ppm NH_3 and 0.88% oxygen with helium as the balance gas. The reaction temperature was varied from 150 to 400°C. The total volumetric flow rate was maintained constant at two different values, 100 cm^3 (STP)/min and 120 cm^3 (STP)/min. The total surface area in the reactor was kept constant. Experiments were also performed to keep the NH_3 conversion level constant by varying the residence time in the reactor. Care was taken to ensure that external and internal mass transfer limitations did not exist. This was verified experimentally as well as by applying the criteria proposed in the literature for mass transfer limitations (*28*). Blank reactor runs were also performed to test the activity of the reactor or the presence of any homogeneous reactions in the absence of the catalyst bed. The results obtained from kinetic experiments were reproducible within 4–5%. The nitrogen balance closures were higher than 96%.

Temperature-Programmed Reduction/Desorption (TPR/TPD)

The TPR/TPD system used for these studies is shown in Fig. 1. A U-shaped quartz sample cell measured 6-mm O.D. by 4-mm I.D. Quartz wool was placed at both sides of the sample layer to fix the solids in place. The cell was heated by a furnace (TECO Manufacturing Company, Model F-6-1100-VH-2-SR), which was mounted on a height-adjustable lab lift (Fisher). A chromel–alumel type-K thermocouple (Omega) was placed in the center of the sample bed. The temperature was programmed, controlled, and displayed by a TECO-SIGMA temperature controller (Model MDC10-RS232). The top of the furnace was covered with an insulated ceramic cap to stabilize the temperature in the furnace.

There were up to eight channels available for gas feeds. Either N_2 or He was used as the TCD reference gas, depending upon the application. Each gas flow rate was controlled by a mass flow controller (Tylan Model FC-280), and displayed on a readout box (Tylan Model RO-28). Before entering the mass flow controller, each gas first passed through a section of $\frac{1}{2}''$ tubing packed with silica gel or molecular sieve 4A to absorb water, then, except O_2, through an oxygen trap (Fisher) to absorb trace amounts of O_2. The uniform mixture from the manifold was sent either to the reactor as in the steady-state option and the pretreatment experiment or through the 6-port valve to vent as in the pulse operation. The three different

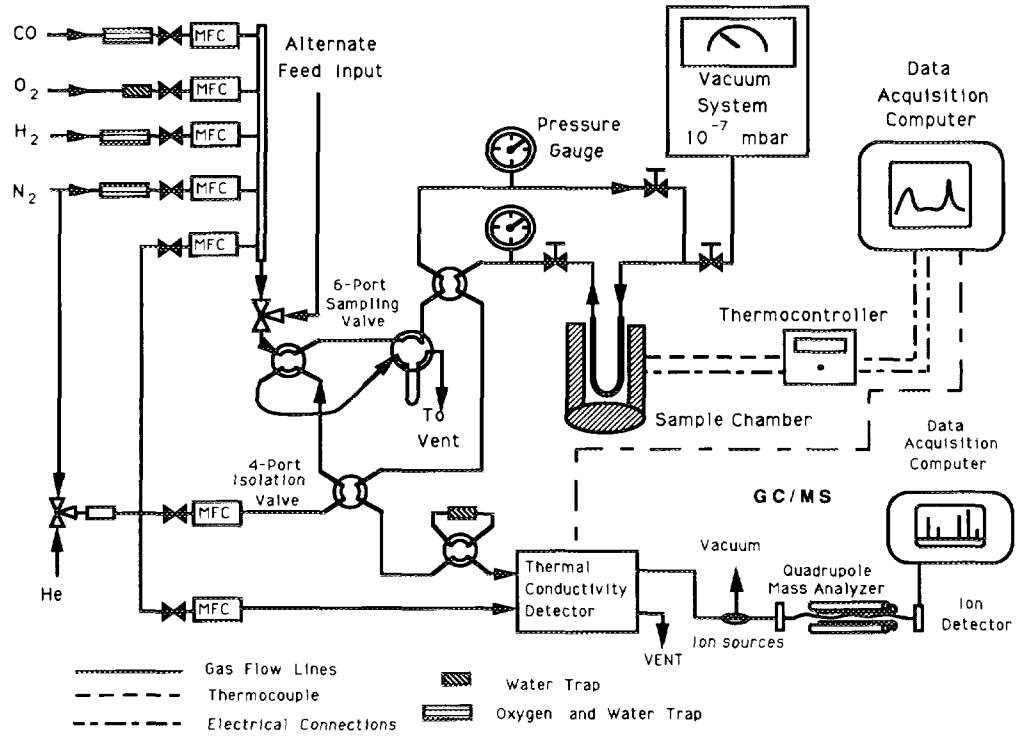

FIG. 1. Flow diagram for the temperature-programmed reduction/desorption system.

options, i.e., steady-state, pulse, and pretreatment, were achieved by a combination of three 4-port valves and one 6-port valve. A 3-way valve was placed right after the manifold. By switching the 3-way valve, a feed mixture from an outside manifold could also be introduced. A vacuum system (ALCATEL) was attached to the sample cell through a $\frac{1}{4}$" flexible tubing to degas the sample *in situ* up to 10^{-7} mbar. Products were analyzed by either a thermal conductivity detector (TCD) or a gas chromatograph–mass spectrometer (Hewlett–Packard, MS Engine, 5989A) or both. In TPR experiments which used ammonia as the reducing agent, it was necessary to use a pulse technique to prevent damage to the mass spectrometer detector due to continuous flow of a stream with high concentrations of ammonia (6.37%). The temperature-programmed furnace, the 6-port valve, and the data recording were all controlled and processed by a Zenith personal computer.

Before TPR experiments, the sample was degassed *in situ* at 400°C for 2 h. The reducing agent was either 6% H_2 in N_2 or 6.37% NH_3 in He. The feed flow rate was set at 60 cm^3(STP)/min. The sample was heated either at 5°C/min or at 2°C/min from 200 to 950°C. The amount of sample was kept constant at either 50 or 400 mg. The volume of the sample bed was kept constant with the aid of quartz particles having the same mesh size as catalyst samples. In order to investigate the nature of reduction intermediates, the experiments were repeated by terminating the process after each TPR peak by cooling and flowing He or N_2 instead of the reducing agent over the sample. X-ray diffraction and laser Raman spectroscopy were used to identify these intermediates.

Oxygen and NO adsorption were also examined through pulse experiments using 10% O_2 in He and 0.477% NO in He, respectively. The samples were degassed for 2 h at 400°C prior to the pulse experiments. The

samples were subjected to 20 pulses, each pulse of 1 cm^3, the time interval between the pulses being 3.5 min. The pulse was carried by a helium stream, which had a flow rate of 30 cm^3(STP)/min, to the TCD.

Temperature-programmed desorption (TPD) experiments were performed over both samples. The amount of catalyst used was 75 mg for experiments where equal weights of samples were used. TPD experiments were repeated by using an equal total surface area of each sample in the reaction chamber. The sample was degassed *in situ* at 250°C in vacuum for 1 h and then cooled down to room temperature. After the pretreatment, the sample was exposed to a 6.37% NH_3 in He stream for one hour at a flow rate of 30 cm^3(STP)/min at room temperature. Subsequently a pure He stream was introduced to flush the lines for 1 h. The sample was then heated to 680°C at a rate of 15°C/min in a 50 cm^3(STP)/min He stream. The products of desorption were detected by both thermal conductivity and mass spectrometer detectors which were connected in series.

Blank runs were performed for all the temperature-programmed experiments mentioned above.

RESULTS

Catalyst Characterization

The preferred exposure of (010) basal plane and side planes on the V_2O_5 samples was verified by the different characterization techniques applied. The scanning electron microscopy combined with a 3-D imaging technique showed that V_2O_5-D consisted of thick and chunky crystals with roughly equal basal and side planes, while V_2O_5-M consisted of thin, long and sheet-like crystals with the basal plane being the predominant face. These observations were confirmed by XRD studies which showed a much higher relative intensity for diffraction bands resulting from (0*k*0) planes in V_2O_5-M. Raman spectroscopy, on the other hand, showed a higher relative intensity of the band at 995 cm^{-1}, which is associated with V=O stretching vibration, as opposed to the bands at 702, 528, and 483 cm^{-1}, which are associated with bridging oxygen sites (*29*) in the same sample. The details of these characterization results have been presented elsewhere (*17*).

Reaction Studies

The stainless-steel reactor and the quartz wool were tested for catalytic activity by performing blank reactor runs at temperatures varying from 150 to 400°C. The conversion of ammonia was zero up to a temperature of 350°C. It was around 5–6% at 400°C.

Catalytic ammonia oxidation experiments were performed over the same temperature range using both V_2O_5-D and V_2O_5-M catalysts. The reaction parameters were kept the same for ammonia oxidation and SCR reaction experiments to facilitate combination of the two studies in drawing conclusions for the role of ammonia oxidation in the SCR reaction network. The catalyst which had a larger percentage of the side planes exposed, V_2O_5-D, was practically inactive at temperatures below 300°C, and V_2O_5-M was inactive at temperatures below 250°C. N_2, NO, and N_2O were the three nitrogen-containing products of ammonia oxidation. NO_2 formation was not observed under the experimental conditions used in these runs. The ammonia conversion rates and the net NO, N_2, and N_2O formation rates are presented in Figs. 2 and 3 for two different residence times. While the ammonia conversion rates were seen to increase with temperature over both catalysts as expected, V_2O_5-M was found to be more active than V_2O_5-D, on an equal-surface-area basis, over the whole temperature range for both flow rates. The total flow rate did not seem to affect the product distribution significantly. Nitrogen was the main product over both samples. However, the production rate of nitric oxide was higher than that of nitrogen at 400°C over V_2O_5-M in both flow rates. Rate of NO formation showed a very sharp increase from 350 to 400°C over V_2O_5-M. In contrast, the increase in NO

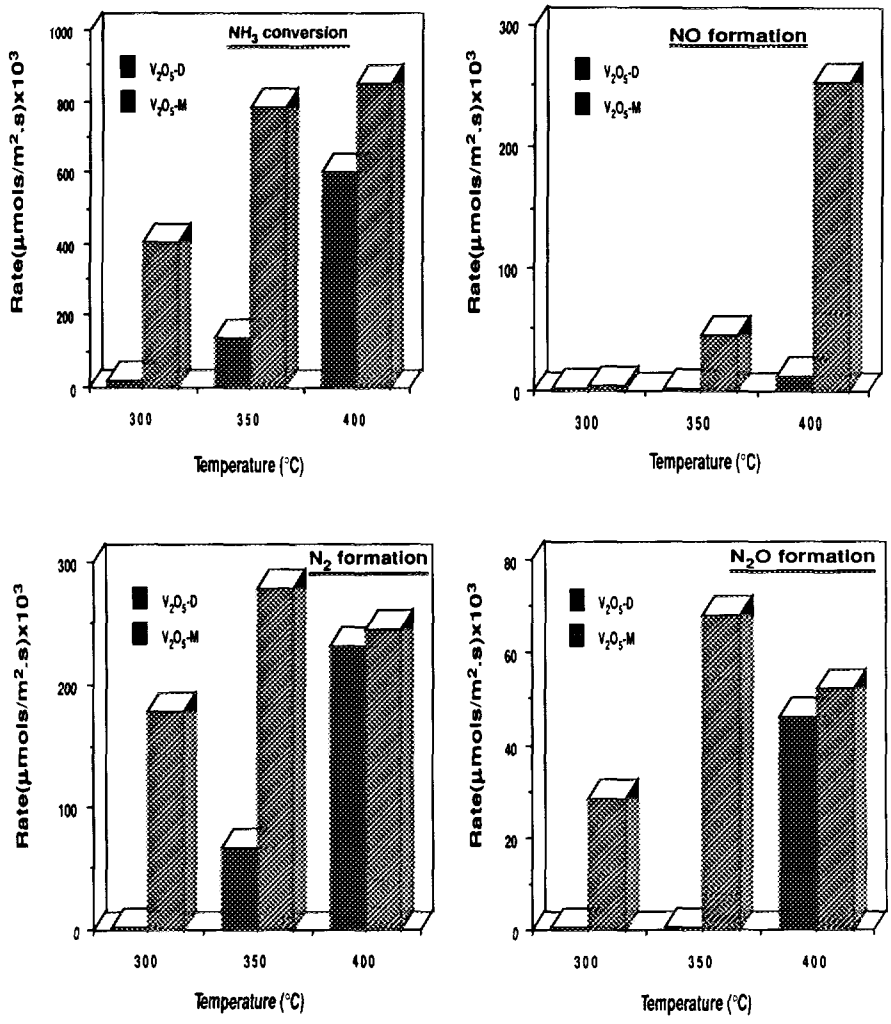

FIG. 2. Comparison of ammonia conversion and product formation rates over V_2O_5-D and V_2O_5-M (total flow rate, 120 cm^3(STP)/min).

formation rate with temperature was much more gradual over V_2O_5-D. The N_2 formation was substantial over V_2O_5-M at all temperatures. However, it showed a fivefold increase over V_2O_5-D from 350 to 400°C. Substantial amounts of N_2O were formed at all temperatures over V_2O_5-M. Over V_2O_5-D, comparable amounts of N_2O were detected only at high temperatures.

The product selectivities over the two catalyst samples were also compared at equal conversion levels. Kinetic measurements were performed at constant ammonia conversion by varying the residence time in the reactor. Figure 4 shows the N_2, N_2O, and NO selectivities at 400°C at an ammonia conversion of 95%. The selectivities for nitrogen and nitrous oxide are higher over V_2O_5-D than V_2O_5-M. The selectivity for nitric oxide, however, is higher over V_2O_5-M.

Temperature-Programmed Reduction/Desorption (TPR/TPD)

The hydrogen TPR profiles of samples V_2O_5-D and V_2O_5-M are shown in Fig. 5. The TPR profile of V_2O_5-D consisted of

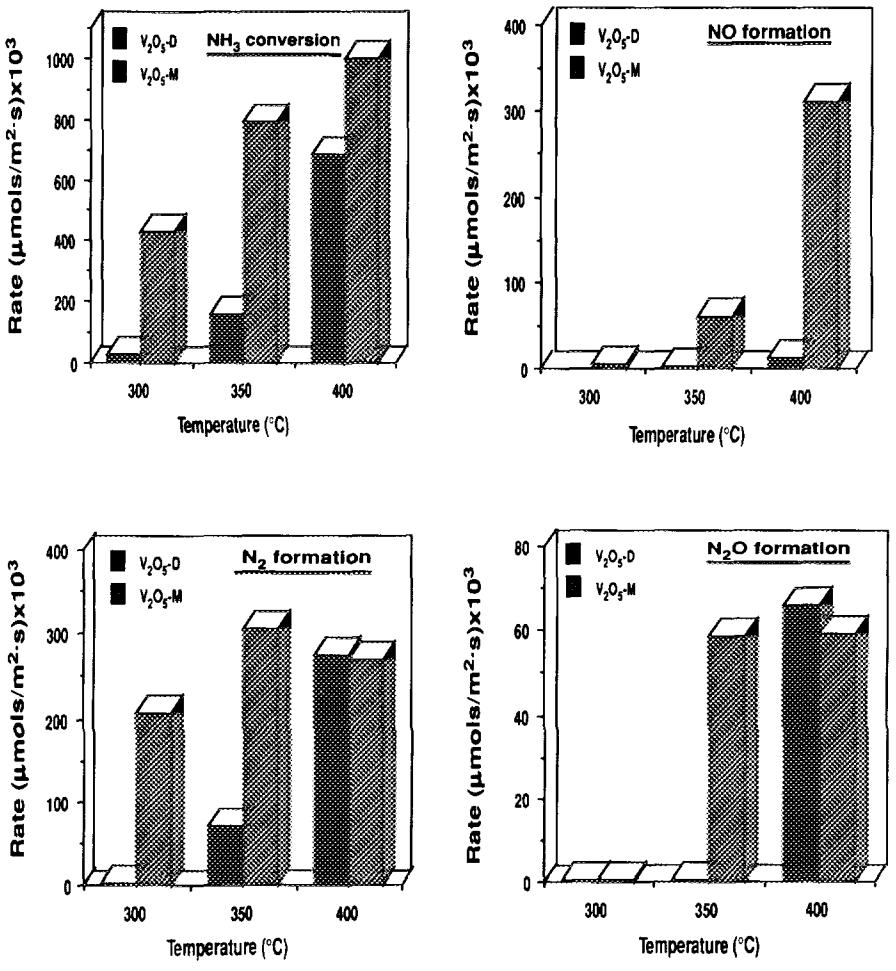

FIG. 3. Comparison of ammonia conversion and product formation rates over V_2O_5-D and V_2O_5-M (total flow rate, 100 cm^3(STP)/min).

three temperature maxima appearing at 660, 690, and 850°C. The XRD technique showed that the first temperature maximum at 660°C was due to reduction of V_2O_5 to V_6O_{13}, while the second and the third maxima at 690 and 850°C were due to further reduction to VO_2 and V_2O_3, respectively. The temperature programmed reduction of V_2O_5-M showed major differences in the profile. There were four features observed appearing at 430, 670, 696, and 870°C. X-ray diffraction showed each stage to consist of a mixture of two vanadium oxide phases. After the first broad temperature maximum, the sample was shown to consist of mostly V_2O_5 with trace quantities of V_6O_{13}. The intermediates identified after the second and third maxima at 670 and 696°C were V_6O_{13} + VO_2 and VO_2 + V_8O_{15}, respectively. V_2O_5-M was also seen to reduce to V_2O_3 at the last stage similar to V_2O_5-D. All of the XRD results were confirmed by the quantification of the hydrogen consumption during the process, as summarized in Table 1.

The temperature-programmed reduction with ammonia as the reducing agent was also performed analyzing the effluent stream by a mass spectrometer. A comparison of the NH_3 TPR profiles is presented in Fig. 6. Because of the slower heating rate and

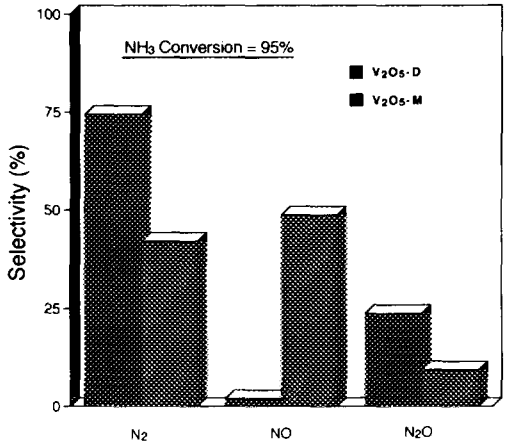

FIG. 4. Comparison of selectivities at equal ammonia conversion of 95%.

TABLE 1

Temperature-Programmed Reduction of V_2O_5 with Hydrogen

V_2O_5-D			V_2O_5-M		
T (°C)	$\%H_2$	Species	T (°C)	$\%H_2$	Species
			430	15.0	$V_2O_5 + V_6O_{13}$
660	33.5	V_6O_{13}	670	30.5	$V_6O_{13} + VO_2$
690	17.7	VO_2	696	14.4	$VO_2 + V_8O_{15}$
850	48.8	V_2O_3	870	40.1	V_2O_3
Total H_2 consumed (mmol/g-V_2O_5)					
11.4			11.0		
Theoretical H_2 requirement					
$V_2O_5 \rightarrow V_2O_3$ 10.99 mmol/g-V_2O_5					

$$V_2O_5 \xrightarrow{33\%} V_6O_{13} \xrightarrow{17\%} VO_2 \xrightarrow{12.5\%} V_8O_{15} \xrightarrow{37.5\%} VO_2$$

larger sample size used, the resolution is lower in these profiles compared to the hydrogen TPR profiles. Both catalysts show two major temperature maxima. Another interesting point to note is the increasing ammonia consumption at higher temperatures. The profiles for the NH_3 TPR products are shown in Figs. 7 and 8 for V_2O_5-D and V_2O_5-M, respectively. There were two nitrogen peaks appearing at 430 and 470°C, and one nitrous oxide feature at 430°C over V_2O_5-M. There was no nitrous oxide produced over V_2O_5-D, although two similar nitrogen peaks were observed at 420°C and 460°C. No nitric oxide was formed on either of the two samples. The ammonia consumption signals shown in Fig. 6 agreed very closely with the trends of the corresponding profiles for nitrogen and nitrous oxide, re-

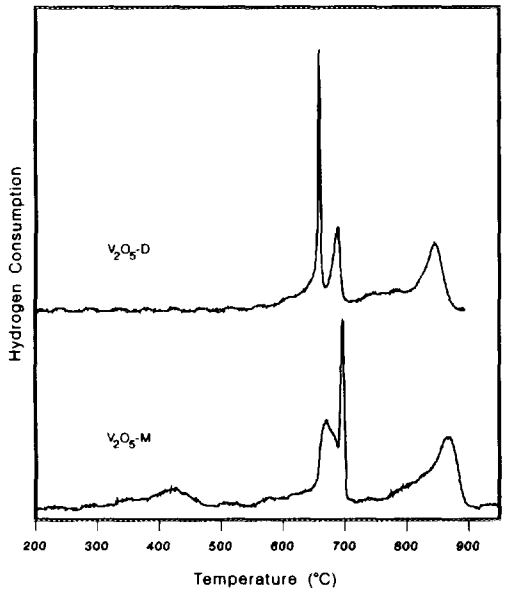

FIG. 5. Comparison of hydrogen TPR profiles over V_2O_5-D and V_2O_5-M (heating rate, 5°C/min).

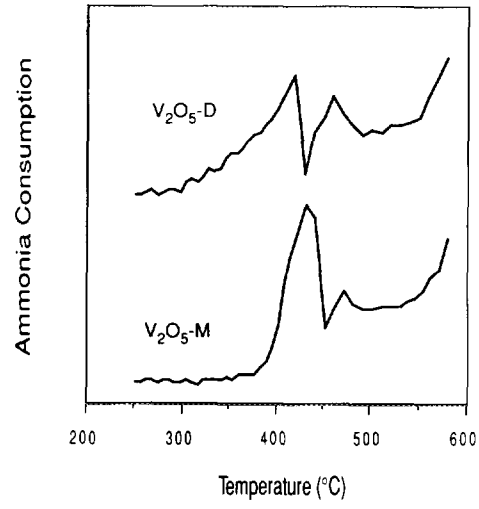

FIG. 6. Comparison of ammonia TPR profiles over V_2O_5-D and V_2O_5-M (heating rate, 2°C/min).

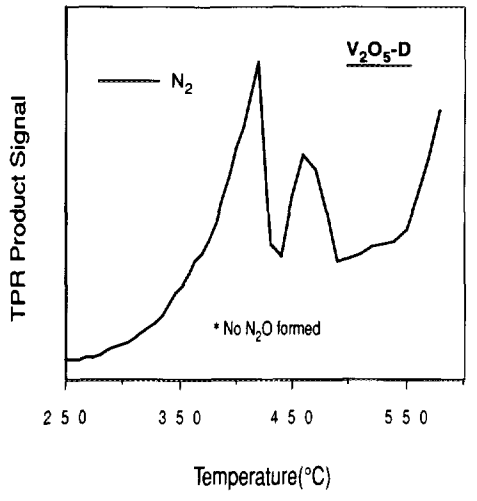

FIG. 7. Product signal profiles in ammonia TPR over V_2O_5-D.

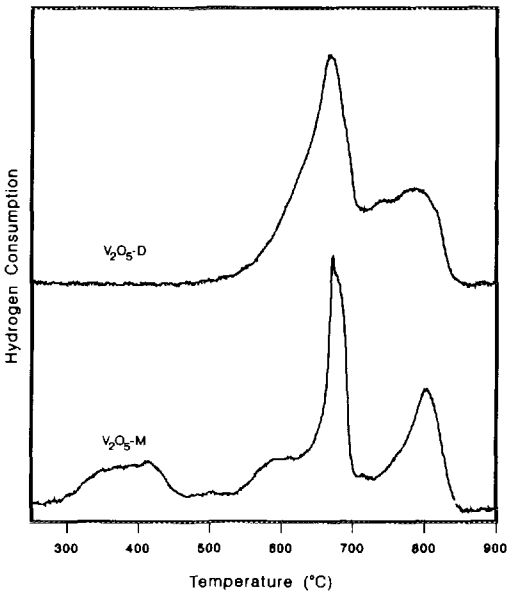

FIG. 9. Comparison of hydrogen TPR profiles over V_2O_5-D and V_2O_5-M (heating rate, 2°C/min).

sulting in a nitrogen balance of almost 100%. XRD analysis over both samples showed that VO_2 was formed after the first reduction peak, and V_2O_3 was formed after the second peak. At temperatures above 520°C, similar to the ammonia consumption, nitrogen signals also kept increasing over both catalysts although there was no longer any water forming. This is an indication of the decomposition of ammonia over the reduced samples (i.e., V_2O_3) resulting in the formation of N_2 and H_2. At temperatures of 660°C and above, ammonia was completely decomposed to N_2 and H_2. A blank run was also performed to examine the decomposition of ammonia in the absence of a catalyst. It was found that the homogeneous ammonia decomposition was not significant until a temperature of 800°C was reached. The ammonia conversion observed due to homogeneous decomposition was less than 10% at 875°C.

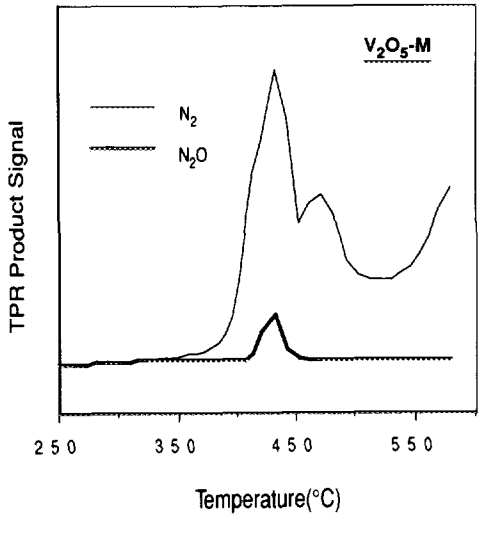

FIG. 8. Product signal profiles in ammonia TPR over V_2O_5-M.

Figure 9 shows the hydrogen TPR profiles of the two vanadium pentoxide samples with the parameters used for ammonia TPR experiments in order to make a reasonable comparison. A low heating rate has to be used in ammonia TPR runs due to the longer time interval required in the pulse technique. Over V_2O_5-D, two maxima were observed at 667 and 788°C and were attributed to reduction of the sample to VO_2 and V_2O_3, respectively. Over V_2O_5-M, in addition to the maxima at 672°C and 803°C, which are

TABLE 2

Comparison of Temperature Maxima in NH_3 and H_2 TRP Profiles

Reduced species	V_2O_5-M		V_2O_5-D	
	NH_3	H_2	NH_3	H_2
VO_2	430°C	672°C	420°C	667°C
V_2O_3	470°C	803°C	460°C	788°C

indicative of reduction to VO_2 and V_2O_3, another broad feature was also observed centered at 412°C. Comparisons of hydrogen and ammonia TPR results are summarized in Table 2.

Adsorption pulse experiments with oxygen and nitric oxide over the calcined samples of V_2O_5-D and V_2O_5-M did not show any significant adsorption.

Experiments examining the temperature-programmed desorption (TPD) of ammonia were performed by combining thermal conductivity and mass spectrometer detectors in series. When the TPD profiles obtained from thermal conductivity detector or the total ion signals obtained from mass spectrometer were examined, there were three features observed over V_2O_5-D, appearing at 160, 410, and 660°C. The TPD profile of V_2O_5-M also had three features, the first one at 130°C, the last one at 660°C. The peak in the middle, however, showed two maxima, not completely resolved, at 380 and 465°C.

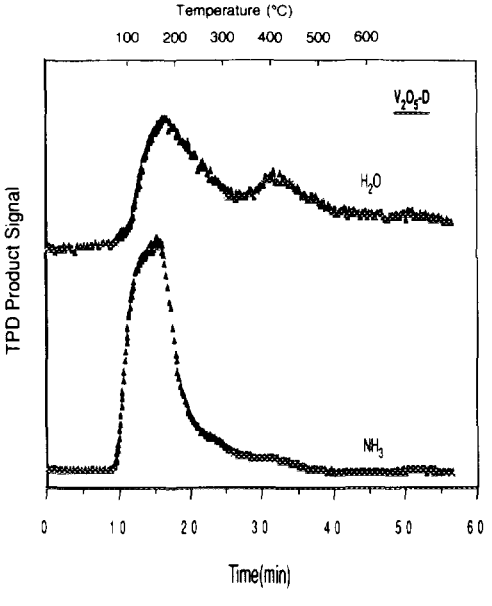

FIG. 10. TPD profiles for NH_3 and H_2O over V_2O_5-D.

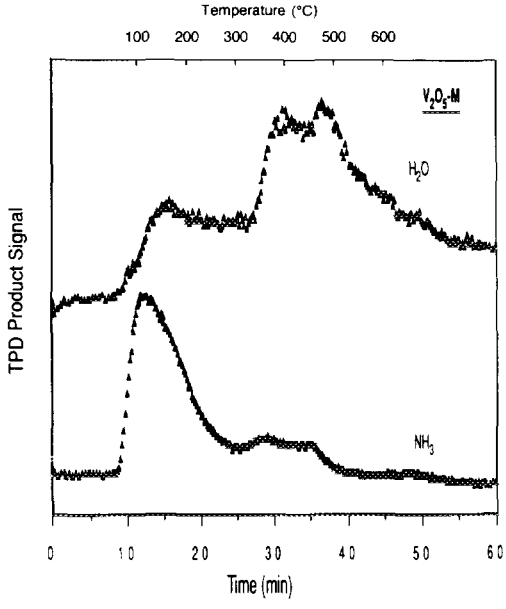

FIG. 11. TPD profiles for NH_3 and H_2O over V_2O_5-M.

Product desorption profiles for water, ammonia, nitrogen, nitric oxide, and nitrous oxide obtained using ion chromatographs are shown in Figs. 10–13. Ammonia profiles show a predominant feature in the low-temperature region. Over V_2O_5-D, NH_3 desorption signal drops down to zero after a shoulder-like feature around 300°C, whereas V_2O_5-M continues to show small quantities of NH_3 desorption at higher temperatures in the form of two small maxima (Figs. 10 and 11). The profiles for water (Figs. 10 and 11) over the two samples look similar in the low-temperature region with maxima appearing at 178 and 157°C for V_2O_5-D and V_2O_5-M, respectively. In the mid-temperature range, however, the pro-

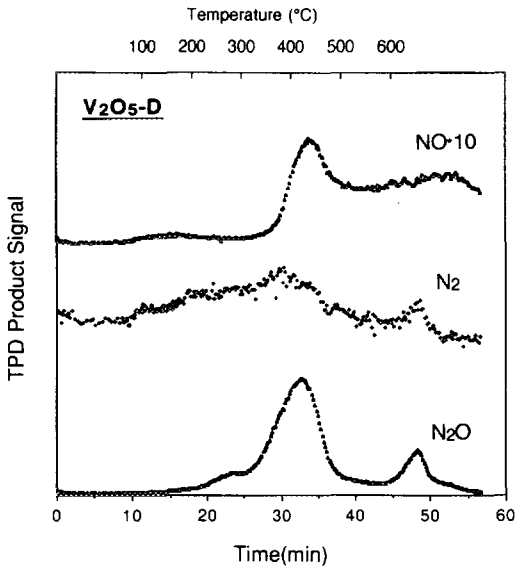

FIG. 12. TPD profiles for N_2, NO, and N_2O over V_2O_5-D.

files are somewhat different, with V_2O_5-M exhibiting two strong maxima at 388 and 459°C, while V_2O_5-D exhibits one weak maximum at 410°C. Profiles for nitrogen, nitric oxide, and nitrous oxide for V_2O_5-D and V_2O_5-M are shown in Figs. 12 and 13, respectively. Nitrogen profiles show substantial quantities of N_2 forming over V_2O_5-M with maxima appearing at 350, 447, and 658°C, while nitrogen signal from V_2O_5-D is weaker, with maxima appearing at 366 and 658°C. The profile for N_2O shows maxima at 350, 447, and 658°C over V_2O_5-M. Over V_2O_5-D, there are two maxima at 426 and 658°C. There is also a shoulder-like feature at 280°C. The TPD profile for NO shows temperature maxima at 430 and 658°C for V_2O_5-M and at 445 and 658°C for V_2O_5-D. The intensity of the N_2O signal is higher for V_2O_5-M in the mid-temperature region, however, the same signal for V_2O_5-D is higher in the high-temperature region. Another interesting feature of the ammonia TPD experiments was the presence of small quantities of oxygen observed over V_2O_5-D at temperatures above 650°C.

DISCUSSION

Ammonia oxidation and thermal analysis studies performed over vanadium pentoxide crystals preferentially exposing different crystal faces showed important differences in their reduction, adsorption, and desorption behavior as well as the product distribution observed in ammonia oxidation. When the observations made in this study are combined with the results from our earlier studies (*17*) on selective catalytic reduction of NO over the same catalysts, they provide important clues about the catalytic role played by different sites in SCR reactions and direct ammonia oxidation reactions over the vanadia catalysts.

Characterization experiments which combined SEM, three-dimensional imaging, X-ray diffraction, XPS, and laser Raman spectroscopy showed that the two vanadium pentoxide samples were identical in chemical structure, but showed considerable differences in the way the crystals were grown. While one of the samples, V_2O_5-M, exposed a larger percentage of the (010) basal plane by growing parallel to the (*ac*)

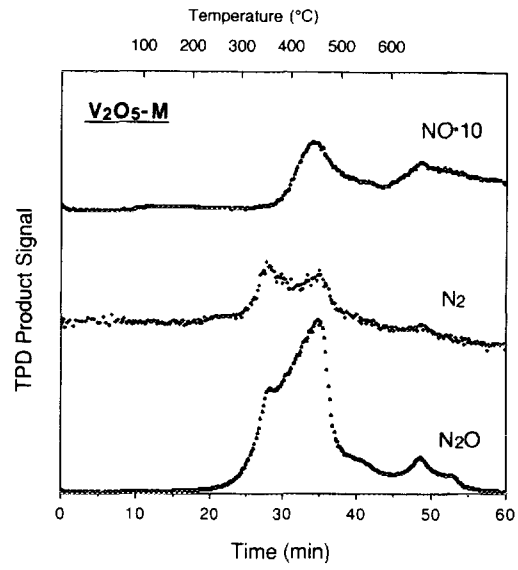

FIG. 13. TPD profiles for N_2, NO, and N_2O over V_2O_5-M.

plane, the second gave rise to crystals that grew in all three dimensions more uniformly, thus leading to larger percentages of the side plane (100) exposure (V_2O_5-D). The ratios of basal plane to side plane area were in the range of 1.5–1.9 and 9.5–10.7 for V_2O_5-D and V_2O_5-M, respectively. Another important difference between the two samples was the difference in the relative intensity of the Raman bands that were associated with V=O sites versus bridging oxygen sites, with V_2O_5-M exhibiting a larger abundance of the terminal oxygen sites (*17*).

Various thermal analysis techniques applied to the vanadium pentoxide catalysts gave important clues about the nature of sites present on the different planes of these crystalline materials. Hydrogen TPR profiles showed a greater reducibility of the samples which preferentially exposed the (010) plane. As reported in the literature (*30*), reduction intermediates were V_6O_{13}, VO_2, and V_2O_3 over both samples. However, V_2O_5-M exhibited a unique feature which was a broad maximum in the 410–430°C range. This broad feature, which was observed at low temperatures over V_2O_5-M, but was absent over V_2O_5-D suggests a surface reduction phenomenon which could conceivably be proceeding through terminal oxygen sites on this sample. Although the XRD technique indicated that a very small amount of V_6O_{13} was present after this first temperature maximum, the reduction was still restricted to the surface. The reason the reduction at this low temperature gives rise to a substantial amount of hydrogen consumption although the signal for the formation of second reduced phase is still minimal could be due to the rapid diffusion of lattice oxygen to terminal oxygen sites located on the basal plane. The absence of the low-temperature feature over V_2O_5-D could be due to the lower reducibility of the bridging oxygen sites or due to a slower rate of solid state diffusion of lattice oxygen to the sites on the side planes. Anisotropy of lattice oxygen diffusion could be one of the complementary factors leading to the catalytic anisotropy over these crystals.

Once the bulk reduction becomes significant, the amounts of hydrogen consumption in each peak (Table 1) over V_2O_5-D were quite close to the theoretical hydrogen requirements for reduction to V_6O_{13}, VO_2, and V_2O_3 phases. This agreement indicated that a nearly pure vanadium oxide phase was formed after each reduction step over V_2O_5-D, as confirmed by the XRD technique. Both XRD technique and hydrogen consumption calculations showed that over V_2O_5-M a new vanadia phase starts to form before the previous phase disappears completely. The total amount of H_2 consumed to reduce V_2O_5 to V_2O_3 agreed quite closely with the theoretical value of 10.99 mmol/g over both catalysts.

Lowering the temperature ramp rate and increasing the sample amounts (Figs. 5 and 9) resulted in a poorer resolution for the profiles. However, the broad feature over V_2O_5-M persisted though the center was shifted to lower temperatures.

Using ammonia in TPR experiments has higher relevancy to the SCR and ammonia oxidation reactions, since ammonia is the most widely used reducing agent in SCR processes (*31*). Ammonia TPR results showed two maxima over both catalysts for ammonia consumption which corresponded to the formation of VO_2 and V_2O_3. The rise in ammonia consumption was more gradual on V_2O_5-D as opposed to the sharper increase over V_2O_5-M. The nitrogen signal obtained from the TPR process also gave rise to two maxima. One major difference between the two catalysts was the absence of any N_2O signal over V_2O_5-D. Interestingly there is no nitric oxide observed in TPR process, in contrast to the TPD runs. As reported in literature (*26*), NO is a possible intermediate in ammonia oxidation reaction. It is possible that the constant flow of ammonia converted all of NO produced in the process to N_2 by NO + NH_3 reaction over V_2O_5-D, and part of it was converted

to N_2O over the basal planes of V_2O_5-M, as was the case in SCR reaction experiments (*17*). A broad feature over V_2O_5-M, which appeared in hydrogen TPR, was not observed in the process of ammonia TPR. This can be explained by the fact that ammonia is a stronger reducing agent than hydrogen and the surface/subsurface reduction which was maintained for a considerable length of time in hydrogen reduction with rapid oxygen diffusion from the bulk to the V=O sites on the basal planes, was not maintained in case of NH_3 reduction because of the stronger reducing ability of ammonia. Subsequently, the catalyst sample was ready to undergo bulk reduction/phase transformation before any substantial ammonia consumption due to surface/subsurface reduction of the basal plane could be detected.

When the two reducing agents, hydrogen and ammonia, are compared, we see that ammonia is a stronger reducing agent than hydrogen. Temperatures required to reduce V_2O_5 to VO_2 with hydrogen were about 250°C higher than those required with NH_3 (Table 2). Similarly, the process with H_2 required temperatures about 330°C higher than those with NH_3 for further reduction to V_2O_3.

Another interesting feature of the NH_3 TPR experiments was the evidence obtained for the decomposition of ammonia. At temperatures 520°C and above nitrogen signals started to increase along with an increase in the hydrogen signal. The water signal, however, disappeared completely. At temperatures 660°C and above, all of the ammonia was converted to N_2 and H_2. The blank runs performed using the same experimental parameters showed the ammonia decomposition activity to be below 10%, even at temperatures as high as 875°C, indicating that the ammonia decomposition reaction was not occurring homogeneously but was catalyzed by the V_2O_3 phase which is the dominant structure above 500°C in NH_3 TPR process.

Thermal desorption experiments with NH_3 provided important clues about the nature of sites for ammonia adsorption and the role of lattice oxygen in ammonia oxidation reactions. The amounts of ammonia and water desorbed over V_2O_5-D to V_2O_5-M at temperatures below 160°C are about equal for the two catalysts when the comparison is based on signals normalized with respect to surface area. This suggests that ammonia and water desorbing at these low temperatures are not site-specific and attached to the surface through weak bonding. Considering that the desorption temperature for these species in the first peak is well below the reaction temperature at which any significant amount of ammonia oxidation takes place, this desorption feature is rather irrelevant for ammonia oxidation.

The second TPD feature which appears between the temperatures of 380 and 465°C has more relevancy for ammonia oxidation since it exhibits the presence of ammonia oxidation products and is much more prevalent than the third feature, which appears at temperatures above 650°C. While on V_2O_5-M, N_2, H_2O, and N_2O peaks are partly resolved in this mid-temperature feature, NO peak has only one temperature maximum, suggesting that in this temperature range there is only one type of site which is leading to NO formation, whereas N_2 and N_2O formation is governed by two types of sites or possibly two different reaction schemes involving two different sites. In the mid-temperature feature the main nitrogen species is N_2O. We also see more desorption products over V_2O_5-M in the mid-temperature range.

The high-temperature features which occur around 655°C in N_2 and N_2O desorption profiles are more dominant over V_2O_5-D than they are over V_2O_5-M. N_2O is still the major species in this temperature range although NO and N_2 are present in small quantities. The relative intensity of NO signal in the high temperature range is higher for V_2O_5-D than it is for V_2O_5-M. Also desorbing at this temperature over V_2O_5-D is a small quantity of molecular oxygen. Over V_2O_5-M, however, there is no oxygen sig-

nal detected at this temperature. One possible explanation is the higher rate of desorption of oxygen-containing products over V_2O_5-M, leaving this sample with more oxygen vacancies, while V_2O_5-D still has relatively more "surface/subsurface" oxygen that could desorb in the form of molecular oxygen at higher temperatures.

When the signals for individual products are compared by normalizing them with respect to total surface area, there is a larger amount of ammonia oxidation products being formed over V_2O_5-M at lower temperatures whereas at higher temperatures V_2O_5-D has the higher overall desorption rate. Another noteworthy point is the comparison of total NO desorption yields which are about equal when normalized with respect to area of the (010) plane, suggesting that the sites responsible for the initial oxidation of ammonia to NO are located on the (010) planes of the catalyst. It is more difficult to draw the same conclusion for the formation of N_2O and N_2, since these products probably involve more than one site and possibly multiple steps. The ratio of the water produced over V_2O_5-D to that over V_2O_5-M is in agreement with the theoretically calculated ratio considering the reactions producing NO, N_2O, and N_2.

To explain the product distribution in steady-state reaction experiments one has to take into consideration the complex network of reactions occurring in ammonia oxidation (*8, 32*). The possible reactions are:

$$4NH_3 + 3O_2 \rightarrow 2N_2 + 6H_2O \quad (1)$$

$$4NH_3 + 5O_2 \rightarrow 4NO + 6H_2O \quad (2)$$

$$2NH_3 + 2O_2 \rightarrow N_2O + 3H_2O \quad (3)$$

$$4NH_3 + 7O_2 \rightarrow 4NO_2 + 6H_2O. \quad (4)$$

The fact that no NO_2 was observed during our experiments makes the reaction that leads to the formation of NO_2 not as relevant for this study as the other reactions although it has been proposed by some researchers in the literature (*32*). Although decomposition of ammonia and NO are also possible reactions that could take place during ammonia oxidation (*25*), they become significant only at temperatures above 500°C.

Some of the earlier studies (*26*) have reported NO as an intermediate in the formation of N_2 and N_2O from ammonia. Although we don't have evidence that would prove or rule out the possibility of N_2 and N_2O forming directly from interaction of two ammonia molecules, the possibility of multiple paths that could lead to the formation of N_2 and N_2O still remains. If this is the case, then one has to include another set of reactions that involve interaction of NO and ammonia in the reaction scheme to be considered for ammonia oxidation:

$$4NO + 4NH_3 + O_2 \rightarrow 4N_2 + 6H_2O \quad (5)$$

$$4NO + 4NH_3 + 3O_2 \rightarrow 4N_2O + 6H_2O \quad (6)$$

$$NO + 4NH_3 \rightarrow 5N_2 + 6H_2O \quad (7)$$

$$8NO + 2NH_3 \rightarrow 5N_2O + 3H_2O. \quad (8)$$

Our earlier studies (*15*) where role of gas-phase oxygen was examined suggest that under the experimental conditions used in this study no considerable conversion level could be maintained under the steady-state conditions, leading us to conclude that reactions (7) and (8) cannot have played a major role in the reaction scheme.

The trends we saw in this study, when combined with our earlier studies focusing on SCR reactions over the same catalysts, suggest that ammonia oxidation and selective catalytic reduction of NO with ammonia to N_2 take place on different catalytic sites and are governed by different activation energies. We believe that the difference in the temperature sensitivities of the ammonia oxidation and SCR reactions plays a major role in shaping the product distribution. The activation energy of ammonia oxidation reactions was found to be over four times that of NO reduction reaction over V_2O_5/Al_2O_3 catalysts (*5*). If a similar difference exists for the activation energies of ammonia oxi-

dation and SCR reactions over unsupported vanadia catalysts, this can explain some of the trends seen in ammonia oxidation and SCR reactions.

One of the points of controversy in the literature is the location of sites for ammonia adsorption. While some researchers suggest that the ammonia adsorption is restricted to V=O sites (*33*), others suggest that ammonia adsorption leading to NO reduction takes place on the Brønsted acid sites located on the side planes (*20*). Although some of the more recent studies on supported vanadia catalysts (*12*, *34*) provide important insight into the nature of ammonia adsorption sites, it is not always possible to correlate the results obtained from unsupported crystals to those obtained from supported catalysts. Our observations so far lead us to conclude that ammonia is adsorbed on at least two types of sites, one type of site being the V=O sites on the (010) basal plane and the other being the bridging oxygen sites located on the side planes. We believe that ammonia species adsorbed on the V=O site lead to the oxidation of ammonia, and in the presence of NO, to the formation of N_2O. The ammonia species adsorbed on the bridging oxygen sites, however, selectively promote formation of N_2 through interaction with gas-phase NO. Although direct oxidation of NH_3 to N_2 and N_2O cannot be ruled out as a possibility, it is more likely that NO formation is a favored first step in ammonia oxidation, especially at higher temperatures. This, in turn, opens the way for NO + NH_3 reaction which could lead to N_2O and N_2 formation. This possibility can also explain why at equal conversion levels nitrogen is the major product over V_2O_5-D, while V_2O_5-M shows the highest selectivity for nitric oxide.

The NH_3 TPD experiments also provide some evidence that support this possibility. An interesting aspect of the comparison between the high-temperature desorption features for the two catalysts is its similarity to the way the two catalysts behave in ammonia oxidation at higher temperatures. The N_2 and N_2O desorption rates over the two catalysts in the high-temperature range are approximately equal while NO desorption rate is much higher over V_2O_5-M. Similarly, in the NH_3 oxidation experiments, V_2O_5-D and V_2O_5-M are seen to have about equal yields for N_2 and N_2O in the high-temperature region, while the yield for NO is much higher for V_2O_5-M than for V_2O_5-D, again suggesting that NO formation could be a first step in NH_3 oxidation and it could be taking place on the V=O sites preferentially. This observation also leads us to think that it could be the terminal oxygen sites incorporating oxygen into the NH_3 molecule for the formation of NO even in the presence of gas-phase oxygen.

While some of the evidence we have seen in our earlier work (*17*) supports the suggested job distribution among catalytic sites found on V_2O_5 surfaces, the results obtained in this study, in turn, help to explain some of the phenomena observed in our earlier NO reduction experiments. As we have seen in our previous steady-state NO reduction studies, NO and NH_3 conversion rates are close to one another at low temperatures. At higher temperatures, NH_3 conversion rates show a tenfold increase over the catalysts which preferentially expose the basal planes while apparent NO conversion declines. This is not only due to rapid increase in NH_3 consumption through ammonia oxidation, but also partly due to formation of NO in the NH_3 oxidation reaction.

The suggestion that ammonia oxidation takes place predominantly over the sites located on the basal planes is supported when we compare the ammonia conversion rates in ammonia oxidation normalized with respect to surface area of the basal planes. Although the rates based on total surface area makes V_2O_5-M appear to be more active in NH_3 oxidation than V_2O_5-D (0.996 and 0.685 μmol/m^2-s, respectively, at 400°C), when the rates are based on the surface area of the basal plane, the activities of the two catalysts come out to be equal with rates for V_2O_5-D and V_2O_5-M

being 1.092 and 1.089 μmol/m^2-s, respectively.

Another important observation to be made in these studies is related to the role of lattice oxygen. Our NH_3 TPR and TPD studies indicate that lattice oxygen can be incorporated into nitrogen species in SCR and NH_3 reactions, as proposed earlier (*35*). However, in steady-state reactions, it is necessary to have gas-phase oxygen present to maintain the reaction. A possible role played by the gas-phase oxygen is to replenish the reduced oxygen sites although there is also evidence of lattice oxygen diffusion from the bulk to the surface, especially to the V=O sites. Our current studies which involve transient isotopic labeling technique under steady-state reaction conditions will be helpful in elucidating the mechanism for the involvement of gas-phase and lattice oxygen in NH_3 oxidation and NO–NH_3 reaction as well as in examining the mobility of subsurface lattice oxygen.

ACKNOWLEDGMENTS

This material is based upon the work supported by the Environmental Protection Agency under Award R-815861-01-0. Partial financial support from Exxon Corporation is also gratefully acknowledged.

REFERENCES

1. Bosch, H., Janssen, F. J. J. G., van den Kerkhof, F. M. G., Oldenziel, J., van Ommen, J. G., and Ross, J. R. H., *Appl. Catal.* **25,** 239 (1986).
2. Bauerle, G. L., Wu, S. C., and Nobe, K., *Ind. Eng. Chem. Prod. Res. Dev.* **14**(4), 268 (1975).
3. Bauerle, G. L., Wu, S. C., and Nobe, K., *Ind. Eng. Chem. Prod. Res. Dev.* **17**(2), 117 (1978).
4. Morikawa, S., Yoshida, H., Takahashi, K., and Kurita, S., *Chem. Lett.*, 251 (1981).
5. Nam, I-S, Eldridge, J. W., and Kittrell, J. R., *Ind. Eng. Chem. Prod. Res. Dev.* **25,** 186 (1986).
6. Haber, J., Kozlowska, A., and Kozlowski, R., *J. Catal.* **102,** 52 (1986).
7. Inomata, M., Miyamoto, A., Ui, T., Kobayashi, K., and Murakami, Y., *Ind. Eng. Chem. Prod. Res. Dev.* **21,** 424 (1982).
8. Janssen, F. J. J. G., *Kema Sci. Tech. Rep.* **6**(1), 1 (1988).
9. Kotter, M., Lintz, H.-G., Turek, T., and Trimm, D. L., *Appl. Catal.* **52,** 225 (1989).
10. Bond, G. C., and Tahir, S. F., *Appl. Catal.* **71,** 1 (1991).
11. Bosch, H., and Janssen, F., *Catal. Today* **2,** 369 (1988).
12. Went, G. T., Leu, L.-J., Lombardo, S. J., and Bell, A. T., *J. Phys. Chem.* **96,** 2235 (1992).
13. Went, G. T., Leu, L.-J., Rosin, R. R., and Bell, A. T., *J. Catal.* **134,** 492 (1992).
14. Handy, B. E., Maciejewski, M., and Baker, A., *J. Catal.* **134,** 75 (1992).
15. Cai, Y., and Ozkan, U.S., *Int. J. Energy, Environment, Economics* **1**(3), 229 (1991).
16. Cai, Y., and Ozkan, U.S., *Appl. Catal.* **78,** 241 (1991).
17. Ozkan, U. S., Cai, Y., and Kumthekar, M. W., *Appl. Catal. A*, **96,** 365 (1993).
18. Gasior, M., and Machej, T. J., *J. Catal.* **83,** 472 (1983).
19. Andersson, A., *in* "Adsorption and Catalysis on Oxide Surfaces" (M. Che and G. C. Bond, Eds.), p. 381. Elsevier, Amsterdam, 1985.
20. Gasior, M., Haber, J., Machej, T., and Czeppe, T., *J. Mol. Catal.* **43,** 359 (1988).
21. Handforth, S. L., and Tilley, J. N., *Ind. Eng. Chem.* **26**(12), 1287 (1934).
22. Gandhi, H. S., and Shelef, M., *J. Catal.* **40,** 312 (1975).
23. Pignet, T., and Schmidt, L. D., *Chem. Eng. Sci.* **29,** 1123 (1974).
24. Pignet, T., and Schmidt, L. D., *J. Catal.* **40,** 212 (1975).
25. Hickman, D. A., and Schmidt, L. D., *Ind. Eng. Chem. Res.* **30,** 50 (1991).
26. Kosaki, Y., Miyamoto, A., and Murakami, Y., *Bull. Chem. Soc. Jpn.* **52**(2), 617 (1979).
27. Hasenberg, D., and Schmidt, L. D., *J. Catal.* **104,** 441 (1987).
28. Carberry, J. J., "Chemical and Catalytic Reaction Engineering." McGraw–Hill, New York, 1976.
29. Beattie, I. R., and Gilson, T. R., *J. Chem. Soc. (A)*, 2322 (1969).
30. Bosch, H., Kip, B. J., van Ommen, J. G., Gellings, P. J., *J. Chem. Soc. Faraday Trans. 1* **80,** 2479 (1984).
31. Takagi, M., Kawai, T., Soma, M., Onishi, T., and Tamaru, K., *J. Catal.* **50,** 441 (1977).
32. Heck, R. M., Bonacci, J. C., Hatfield, W. R., and Hsiung, H., *Ind. Eng. Chem. Process Des. Dev.* **21,** 73 (1982).
33. Miyamoto, A., Yamazaki, Y., Inomata, M., and Murakami, Y., *J. Phys. Chem.* **85**(16), 2366 (1981).
34. Srnak, T. Z., Dumesic, J. A., Clausen, B. S., Tornqvist, E., and Topsoe, N. Y., *J. Catal.* **135,** 246 (1992).
35. Janssen, F. J. J. G., van den Kerkhof, F. M. G., Bosch, H., and Ross, J. R. H., *J. Phys. Chem.* **91,** 5921 (1987).